Method to integrate full particle orbit in toroidal plasmas

X. S. Wei,[1] Y. Xiao,[1,a)] A. Kuley,[2] and Z. Lin[2]
[1]Institute for Fusion Theory and Simulation, Zhejiang University, Hangzhou, China
[2]Department of Physics and Astronomy, University of California, Irvine, California 92697, USA

(Received 11 February 2015; accepted 10 August 2015; published online 3 September 2015)

It is important to integrate full particle orbit accurately when studying charged particle dynamics in electromagnetic waves with frequency higher than cyclotron frequency. We have derived a form of the Boris scheme using magnetic coordinates, which can be used effectively to integrate the cyclotron orbit in toroidal geometry over a long period of time. The new method has been verified by a full particle orbit simulation in toroidal geometry without high frequency waves. The full particle orbit calculation recovers guiding center banana orbit. This method has better numeric properties than the conventional Runge-Kutta method for conserving particle energy and magnetic moment. The toroidal precession frequency is found to match that from guiding center simulation. Many other important phenomena in the presence of an electric field, such as $E \times B$ drift, Ware pinch effect and neoclassical polarization drift are also verified by the full orbit simulation. © *2015 AIP Publishing LLC*. [http://dx.doi.org/10.1063/1.4929799]

I. INTRODUCTION

Particle-in-cell (PIC) simulation is widely used to study the complicated plasma dynamics,[1] where the position and velocity of charged particles as well as electromagnetic fields are advanced in time simultaneously. It is essential in the PIC simulation to push particle in the phase space accurately. In order to simulate the particle motion in slowly varying electromagnetic fields (with frequency lower than cyclotron frequency), the formulation to push the guiding centers in magnetic coordinates has been developed and greatly advanced the gyrokinetic simulation.[2–5] When the electromagnetic field frequency is comparable or higher than the cyclotron frequency, e.g., the radio frequency electromagnetic waves used for plasma heating and current drive, the full particle orbit, rather than the guiding center orbit needs to be calculated accurately over a very long time scale.[6–9]

Boris algorithm is an outstanding choice to integrate the cyclotron orbit of the charged particle with its time-explicit nature.[10,11] The Boris algorithm conserves phase space volume in non-relativistic limit, making it very attractive in the non-relativistic long-time simulation. The Boris algorithm has been recently found not to conserve phase space volume in the relativistic limit.[12] Qin *et al*. demonstrate that although it conserves phase space volume, the Boris algorithm is not symplectic with finite time step size.[13] However, Webb later reports that the symplectic feature is recovered for the Boris algorithm by expanding the discrete Euler-Lagrange equation to the higher order.[14] The latest publications by Zhang[15] and He[16] tend to confirm Qin's original conclusion. Therefore, whether the Boris algorithm is symplectic or not remains an open issue.

The conventional Boris algorithm works well in the Cartesian and cylindrical coordinates.[17–19] However, the magnetic coordinates are more suited to describe the complicated magnetic geometry and electromagnetic fluctuations in toroidal plasmas. Therefore, it is desirable to work out a Boris scheme in the magnetic coordinates to accommodate the complex physics in the magnetic fusion devices like tokamaks. In addition, this algorithm should be able to handle the particle dynamics in the long time scale, and it needs to be verified by the particle dynamics with or without external electromagnetic waves.

In this paper, we derive a form of the Boris scheme in the magnetic coordinates, which is used effectively to push particles over a long period of time in the toroidal geometry. In Section II, the basic Boris scheme is introduced and the magnetic coordinates are used to advance the particle position. The complication in advancing velocity in the magnetic coordinates is carefully examined in Section III. Section IV shows simulation results for verification of the new Boris formulation, including the bounce motion and toroidal precession of banana orbits, $E \times B$ drift, Ware pinch effect, and neoclassical polarization drift in the absence of high frequency waves. Summary and discussion are provided in Section V.

II. BORIS ALGORITHM AND POSITION ADVANCE IN TOROIDAL GEOMETRY

The motion of a charged particle in electromagnetic fields is given by the following equations:

$$\frac{d\mathbf{x}}{dt} = \mathbf{v}, \tag{1}$$

$$\frac{d\mathbf{v}}{dt} = \frac{e}{m}(\mathbf{E} + \mathbf{v} \times \mathbf{B}). \tag{2}$$

The leap-frog method[1] has been widely used to advance these equations by shifting the position and velocity of the particle by $\Delta t/2$ to make the scheme time-centered

$$\frac{\mathbf{x}^{t+\Delta t/2} - \mathbf{x}^{t-\Delta t/2}}{\Delta t} = \mathbf{v}^t, \tag{3}$$

a)yxiao@zju.edu.cn

$$\frac{\mathbf{v}^{t+\Delta t}-\mathbf{v}^{t}}{\Delta t}=\frac{e}{m}\left(\mathbf{E}+\frac{\mathbf{v}^{t+\Delta t}+\mathbf{v}^{t}}{2}\times\mathbf{B}\right). \tag{4}$$

In Eq. (4), the electric field $\mathbf{E}$ and magnetic field $\mathbf{B}$ are evaluated at the time of $t+\Delta t/2$. We note that Eq. (4) is implicit in time and thus advancing $\mathbf{v}$ is relatively troublesome. However, Boris introduced two intermediate velocities $\mathbf{v}^{-}$ and $\mathbf{v}^{+}$ to make Eq. (4) time-explicit.[10] These two intermediate velocities connect with $\mathbf{v}^{t}$ and $\mathbf{v}^{t+\Delta t}$ through the following equations:

$$\mathbf{v}^{-}=\mathbf{v}^{t}+\frac{e\Delta t}{2m}\mathbf{E}, \tag{5}$$

$$\mathbf{v}^{+}=\mathbf{v}^{t+\Delta t}-\frac{e\Delta t}{2m}\mathbf{E}. \tag{6}$$

Thus, the acceleration of the electric field $\mathbf{E}$ is split into two half-accelerations. Between these two half-accelerations, the velocity vector $\mathbf{v}^{+}$ at the time step $t+\Delta t/2$ can be obtained from $\mathbf{v}^{-}$ by the following vector rotation:

$$\frac{\mathbf{v}^{+}-\mathbf{v}^{-}}{\Delta t}=\frac{e}{m}\left(\frac{\mathbf{v}^{+}+\mathbf{v}^{-}}{2}\times\mathbf{B}\right) \tag{7}$$

which approximates the Lorentz rotation by the magnetic field. We further note that the preceding equation is still in the implicit form. However, it can be further transformed to the following explicit form:[1]

$$\mathbf{v}^{+}=\mathbf{v}^{-}+(\mathbf{v}^{-}+\mathbf{v}^{-}\times\mathbf{t})\times\mathbf{s} \tag{8}$$

with $\mathbf{t}=\frac{\Omega\Delta t}{2}\mathbf{b}$, $\mathbf{s}=\frac{\Omega\Delta t}{1+(\Omega\Delta t/2)^{2}}\mathbf{b}$, the gyro-frequency $\Omega=\frac{eB}{m}$, and unit vector along the magnetic field $\mathbf{b}=\frac{\mathbf{B}}{B}$. Here the symbol e denotes the particle charge. Therefore, the procedure of advancing velocity is separated into three steps: a half-acceleration by the electric field, a rotation of the velocity vector by the magnetic field, and another half-acceleration by the electric field. In the Cartesian coordinates, with $\mathbf{v}=v_x\mathbf{e}_x+v_y\mathbf{e}_y+v_z\mathbf{e}_z$, the time advancing of velocity is straightforward by following Eqs. (5), (6), and (8) in the three fixed orthogonal directions.

For a toroidal system like tokamak, it is usually more convenient to use magnetic flux coordinates (ψ,θ,ζ) rather than the Cartesian coordinates, where $2\pi\psi$ is the poloidal magnetic flux, and ζ and θ are the effective toroidal and poloidal angle, respectively. In the gyrokinetic theory, the velocity $\mathbf{v}$ is decomposed into three components: $v_{||}$, μ, and the phase angle ϕ, where ϕ is an ignorable variable due to the fast gyromotion. Therefore, the guiding center of the particle is pushed in the 5D phase space $(\psi,\theta,\zeta,v_{||},\mu)$ by the guiding center equation of motion, which can be derived from the guiding center Hamiltonian principle.[2] In the full-kinetic (or full particle orbit) simulation, the decomposition of the velocity variable to $(v_{||},\mu,\varphi)$ will lead to numerical difficulties since these variables are defined on a local orthogonal coordinate system which rotates with the particle motion and hence is not fixed in time and space, e.g., the phase angle will rotate along the magnetic field line in a sheared magnetic field even without any particle gyromotion.

The velocity $\mathbf{v}$ is thus decomposed using three covariant basis vectors $\mathbf{e}_i=\frac{d\mathbf{r}}{d\alpha_i}$, with $\alpha_i=\psi,\theta,\zeta$ for $i=1,2,3$, which can be defined by the magnetic coordinates. Then $\mathbf{v}=(v^{\psi},v^{\theta},v^{\zeta})=\sum_{i=1}^{3}v^{\alpha_i}\mathbf{e}_i$, with the contravariant velocity component $v^{\alpha_i}=\mathbf{v}\cdot\nabla\alpha_i$. The contravariant basis vector is defined as $\mathbf{e}^{i}=\nabla\alpha_i$, with $\mathbf{e}^{i}=J^{-1}\varepsilon_{ijk}\mathbf{e}_j\times\mathbf{e}_k$, where ε_{ijk} is the Levi-Civita symbol, $\varepsilon_{ijk}=1$ if the indices (i,j,k) follow an even permutation of $(1,2,3)$; $\varepsilon_{ijk}=-1$ if the indices (i,j,k) follow an odd permutation of $(1,2,3)$; otherwise $\varepsilon_{ijk}=0$. The transformation Jacobian J between the covariant form and contravariant form is $J=\mathbf{e}_1\times\mathbf{e}_2\cdot\mathbf{e}_3$ and $J^{-1}=\mathbf{e}^{1}\times\mathbf{e}^{2}\cdot\mathbf{e}^{3}$. The position advance in the magnetic flux coordinates derived from Eq. (3) takes the form

$$\alpha_i^{\,t+\Delta t/2}=\alpha_i^{\,t-\Delta t/2}+v^{\alpha_i t}\Delta t. \tag{9}$$

Once the new particle position $\alpha_i^{\,t+\Delta t/2}$ is known, the contravariant basis vector $\mathbf{e}^{it+\Delta t/2}$ at this new time step can be computed.

In Sec. III, we show how to evolve from $\mathbf{v}^{t}$ to $\mathbf{v}^{t+\Delta t}$ in the magnetic coordinates following the Boris algorithm.

III. ADVANCE VELOCITY IN TOROIDAL GEOMETRY

Since the particle changes its position with time, the basis vectors $\mathbf{e}^{i}$ and $\mathbf{e}_i$ at the particle position also change with time. In the absence of an inductive field, the electric field can be expressed by an electrostatic potential $\mathbf{E}=-\nabla\phi$. The velocity evolution equation in the Boris scheme, i.e., Eqs. (5) and (6), can be projected onto the three contravariant basis vectors $\mathbf{e}^{it+\Delta t/2}$ for $i=1,2,3$ at the new time step $t+\Delta t/2$. By defining $u^{\alpha_i t}=\mathbf{v}^{t}\cdot\mathbf{e}^{it+\Delta t/2}$, $u^{\alpha_i t+\Delta t}=\mathbf{v}^{t+\Delta t}\cdot\mathbf{e}^{it+\Delta t/2}$, $u^{\alpha_i -}=\mathbf{v}^{-}\cdot\mathbf{e}^{it+\Delta t/2}$, and $u^{\alpha_i +}=\mathbf{v}^{+}\cdot\mathbf{e}^{it+\Delta t/2}$, Eqs. (5) and (6) can be rewritten as

$$u^{\alpha_i -}=u^{\alpha_i t}-\frac{\Omega\Delta t}{2B}\sum_{j=1}^{3}\frac{\partial\phi}{\partial\alpha_j}g^{\alpha_j\alpha_i}, \tag{10}$$

$$u^{\alpha_i t+\Delta t}=u^{\alpha_i +}-\frac{\Omega\Delta t}{2B}\sum_{j=1}^{3}\frac{\partial\phi}{\partial\alpha_j}g^{\alpha_j\alpha_i}, \tag{11}$$

where the metric tensor is defined as $g^{\alpha_j\alpha_i}=\mathbf{e}^{it+\Delta t/2}\cdot\mathbf{e}^{it+\Delta t/2}$. These geometric tensors in the following are evaluated at time step $t+\Delta t/2$. Similarly, we can define the metric tensor $g_{\alpha_i\alpha_j}=\mathbf{e}_i\cdot\mathbf{e}_j$ and $g_{\alpha_i}^{\alpha_j}=\mathbf{e}_i\cdot\mathbf{e}^{j}$. The contravariant component of Eq. (8) gives

$$u^{\alpha_i +}=u^{\alpha_i -}+\mathbf{v}^{-}\times\mathbf{s}\cdot\mathbf{e}^{it+\Delta t/2}+(\mathbf{v}^{-}\times\mathbf{t})\times\mathbf{s}\cdot\mathbf{e}^{it+\Delta t/2}. \tag{12}$$

It is known that the magnetic field in toroidal system can be expressed in both covariant or contravariant form,[2] $\mathbf{B}=\delta\nabla\psi+I\nabla\theta+g\nabla\zeta=q\nabla\psi\times\nabla\theta+\nabla\zeta\times\nabla\psi$, where $q=q(\psi)$ is the safety factor, $\delta=\delta(\psi,\theta)$, $I=I(\psi)$ and $g=g(\psi)$. Thus, the magnetic field can also be written in terms of the basis vectors

$$\mathbf{B} = \sum_{j=1}^{3} B_j \mathbf{e}^j = \sum_{i=1}^{3} B^i \mathbf{e}_i \tag{13}$$

with $B_j = (\delta, I, g)$, $B^i = (0, J^{-1}, q(J)^{-1})$ and the Jacobian $J = \frac{qg+I}{B^2}$. With these notations, Eq. (12) can be further simplified as

$$u^{\alpha_i +} = \left[1 - \frac{\gamma_B}{2}(\Omega\Delta t)^2\right] u^{\alpha_i -} + \gamma_B \frac{(\Omega\Delta t)^2}{2B^2} \sum_{j=1}^{3} B^i B_j u^{\alpha_j -} - \frac{\gamma_B}{J}\frac{\Omega\Delta t}{B} \sum_{j,k,l=1}^{3} \varepsilon_{ijl} B_j g_{\alpha_k \alpha_l} u^{\alpha_k -} \tag{14}$$

with the constant $\gamma_B = \frac{1}{1+(\Omega\Delta t)^{2/4}}$. This equation can be explicitly expressed for each component in the following way:

$$u^{\psi +} = \left[1 - \frac{\gamma_B}{2}(\Omega\Delta t)^2\right] u^{\psi -} + \frac{\gamma_B}{J}\frac{\Omega\Delta t}{B} \sum_{k=1}^{3} (g g_{\alpha_k \theta} - I g_{\alpha_k \zeta}) u^{\alpha_k -}, \tag{15}$$

$$u^{\theta +} = \left[1 - \frac{\gamma_B}{2}(\Omega\Delta t)^2\right] u^{\theta -} + \gamma_B \frac{(\Omega\Delta t)^2}{2B^2}\frac{1}{J}\left(\delta u^{\psi -} + I u^{\theta -} + g u^{\zeta -}\right) + \frac{\gamma_B}{J}\frac{\Omega\Delta t}{B} \sum_{k=1}^{3} \left(\delta g_{\alpha_k \zeta} - g g_{\alpha_k \psi}\right) u^{\alpha_k -}, \tag{16}$$

$$u^{\zeta +} = \left[1 - \frac{\gamma_B}{2}(\Omega\Delta t)^2\right] u^{\zeta -} + \gamma_B \frac{(\Omega\Delta t)^2}{2B^2}\frac{q}{J}\left(\delta u^{\psi -} + I u^{\theta -} + g u^{\zeta -}\right) + \frac{\gamma_B}{J}\frac{\Omega\Delta t}{B} \sum_{k=1}^{3} \left(I g_{\alpha_k \psi} - \delta g_{\alpha_k \theta}\right) u^{\alpha_k -}. \tag{17}$$

The preceding equations can be used to compute $u^{\alpha_i +} (i = 1, 2, 3)$, which then can be further used to compute $u^{\alpha_i t+\Delta t}$ using Eq. (11). However, $v^{\alpha_i t+\Delta t}$ instead of $u^{\alpha_i t+\Delta t}$ is required to evolve ${\alpha_i}^{t+\Delta t/2}$ to ${\alpha_i}^{t+3\Delta t/2}$, with $v^{\alpha_i t+\Delta t} = \mathbf{v}^{t+\Delta t} \cdot \mathbf{e}^{it+\Delta t}$. The basis vector $\mathbf{e}^{it+\Delta t} = \nabla {\alpha_i}^{t+\Delta t}$ remains unknown since ${\alpha_i}^{t+\Delta t}$ has not been evaluated in the Boris scheme. Here we use the following approximation for ${\alpha_i}^{t+\Delta t}$:

$${\alpha_i}^{t+\Delta t} = {\alpha_i}^{t+\Delta t/2} + u^{\alpha_i t+\Delta t}\frac{\Delta t}{2}. \tag{18}$$

It can be shown that this approximation in Eq. (18) does not affect the energy conservation. However, the volume-preserving property of the Boris scheme is no longer satisfied since this approximation introduces an error of order Δt^2 (see the Appendix).

Once ${\alpha_i}^{t+\Delta t}$ is known, $v^{\alpha_i t+\Delta t}$ can be calculated by

$$v^{\alpha_i t+\Delta t} = \sum_{j=1}^{3} u^{\alpha_j t+\Delta t} \mathbf{e}_j{}^{t+\Delta t/2} \cdot \mathbf{e}^{it+\Delta t}. \tag{19}$$

Thus according to Eq. (12), the new position is given by ${\alpha_i}^{t+3\Delta t/2} = {\alpha_i}^{t+\Delta t/2} + v^{\alpha_i t+\Delta t}\Delta t$, for $i = 1, 2, 3$. Then, the velocity variable $\tilde{u}^{\alpha_i t+\Delta t}$ in the next step of velocity evolution needs to know the basis vector $\mathbf{e}^{it+3\Delta t/2}$ rather than $\mathbf{e}^{it+\Delta t/2}$, which can be then obtained by

$$\tilde{u}^{\alpha_i t+\Delta t} = \sum_{j=1}^{3} u^{\alpha_j t+\Delta t} \mathbf{e}_j{}^{t+\Delta t/2} \cdot \mathbf{e}^{it+3\Delta t/2}. \tag{20}$$

Using the preceding procedures, we can advance one full time step in the original Boris scheme. However, in Eqs. (19) and (20) we need to calculate the dot-product of the covariant and contravariant basis vectors at different time steps. It is most convenient for this calculation if we know the transform between $(\alpha_1, \alpha_2, \alpha_3)$ and the Cartesian coordinates (x, y, z), since $\mathbf{e}^i = \frac{\partial \alpha_i}{\partial x}\hat{\mathbf{x}} + \frac{\partial \alpha_i}{\partial y}\hat{\mathbf{y}} + \frac{\partial \alpha_i}{\partial z}\hat{\mathbf{z}}$ and $\mathbf{e}_i = \frac{\partial x}{\partial \alpha_i}\hat{\mathbf{x}} + \frac{\partial y}{\partial \alpha_i}\hat{\mathbf{y}} + \frac{\partial z}{\partial \alpha_i}\hat{\mathbf{z}}$. Note the unit vectors $(\hat{\mathbf{x}}, \hat{\mathbf{y}}, \hat{\mathbf{z}})$ do not change with the particle motion. We note that it is often more convenient to introduce an intermediate toroidal coordinate system $(\beta_i) = (R, Z, \phi)$, and then to find the transformation between the magnetic flux coordinates (α_i) and the toroidal coordinates (β_i). As the transformation between (β_i) and (x, y, z) is straightforward, we can then rewrite Eqs. (19) and (20) in a more specific form

$$u^{\alpha_i,\text{new}} = \sum_{j=1}^{3}\sum_{m=1}^{3}\sum_{n=1}^{3} u^{\alpha_j,\text{old}} \left(\frac{\partial x}{\partial \beta_m}\frac{\partial \beta_m}{\partial \alpha_j}, \frac{\partial y}{\partial \beta_m}\frac{\partial \beta_m}{\partial \alpha_j}, \frac{\partial z}{\partial \beta_m}\frac{\partial \beta_m}{\partial \alpha_j}\right) \times \left(\frac{\partial \alpha_i}{\partial \beta_n}\frac{\partial \beta_n}{\partial x}, \frac{\partial \alpha_i}{\partial \beta_n}\frac{\partial \beta_n}{\partial y}, \frac{\partial \alpha_i}{\partial \beta_n}\frac{\partial \beta_n}{\partial z}\right), \tag{21}$$

where the basis vectors of magnetic coordinate system are expressed using the Cartesian coordinates in order to calculate the dot product in Eq. (19).

It is also interesting to note that Eqs. (19) or (20) can be regarded as a rotation of the basis vectors as the particle moves from one time step to the next time step. Especially, for a locally orthogonal system, the transformation can be greatly simplified. For example, we can find the transformation analytically for tokamaks with a concentric circular cross-section, which is a very useful equilibrium model for

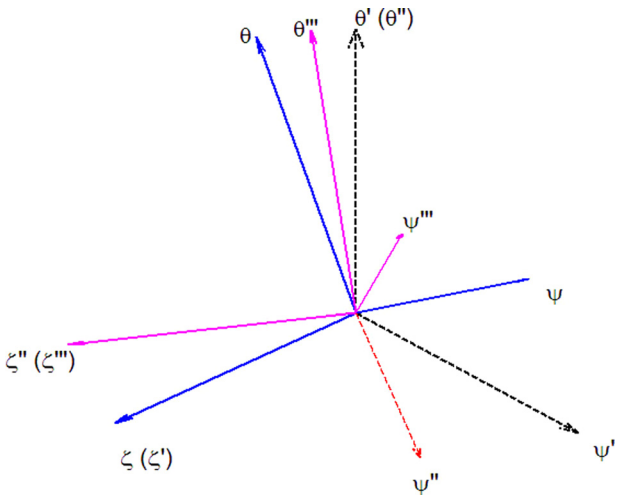

FIG. 1. The rotation of unit basis vectors, $(\hat{\psi}, \hat{\theta}, \hat{\zeta})$ are the initial directions of three unit vectors; $(\hat{\psi}', \hat{\theta}', \hat{\zeta}')$ are the three unit vectors after the first rotation; $(\hat{\psi}'', \hat{\theta}'', \hat{\zeta}'')$ are the three unit vectors after the second rotation; and $(\hat{\psi}''', \hat{\theta}''', \hat{\zeta}''')$ are the three unit vectors after the third rotation.

many applications. When a particle moves from $(\psi_1, \theta_1, \zeta_1)$ to $(\psi_2, \theta_2, \zeta_2)$, the directions of the basis vectors change with time as shown in Fig. 1. This rotation can be separated into three steps: a first rotation about ζ axis by an angle $-\theta_1$, a second rotation about θ' axis by an angle $\Delta\zeta = \zeta_2 - \zeta_1$, and a third rotation about the ζ'' axis by an angle θ_2. Thus, the initial basis vectors can be written by the linear combinations of the final ones

$$\mathbf{e}_\psi^{\text{old}} = \Big\{\mathbf{e}_\psi^{\text{new}}|\nabla\psi_2|[\sin\theta_1\sin\theta_2 + \cos\theta_1\cos\theta_2\cos\Delta\zeta] + \mathbf{e}_\theta^{\text{new}}|\nabla\theta_2|[\sin\theta_1\cos\theta_2 - \cos\theta_1\sin\theta_2\cos\Delta\zeta] - \mathbf{e}_\zeta^{\text{new}}|\nabla\zeta_2|\sin\Delta\zeta\cos\theta_1\Big\}\frac{1}{|\nabla\psi_1|}, \tag{22}$$

$$\mathbf{e}_\theta^{\text{old}} = \Big\{\mathbf{e}_\psi^{\text{new}}|\nabla\psi_2|[\cos\theta_1\sin\theta_2 - \sin\theta_1\cos\theta_2\cos\Delta\zeta] + \mathbf{e}_\theta^{\text{new}}|\nabla\theta_2|[\cos\theta_1\cos\theta_2 + \sin\theta_1\sin\theta_2\cos\Delta\zeta] + \mathbf{e}_\zeta^{\text{new}}|\nabla\zeta_2|\sin\Delta\zeta\sin\theta_1\Big\}\frac{1}{|\nabla\theta_1|}, \tag{23}$$

$$\mathbf{e}_\zeta^{\text{old}} = \Big[\mathbf{e}_\psi^{\text{new}}|\nabla\psi_2|\cos\theta_2\sin\Delta\zeta - |\nabla\theta_2|\mathbf{e}_\theta^{\text{old}}\sin\theta_2\sin\Delta\zeta + |\nabla\zeta_2|\mathbf{e}_\zeta^{\text{old}}\cos\Delta\zeta\Big]\frac{1}{|\nabla\zeta_1|}. \tag{24}$$

The velocity does not change with the basis vectors, i.e.,

$$\mathbf{v} = \sum u^{i,\text{old}}\mathbf{e}_i^{\text{old}} = \sum u^{i,\text{new}}\mathbf{e}_i^{\text{new}}. \tag{25}$$

The new components of velocity can then be written as

$$u^{\psi,\text{new}} = |\nabla\psi_2|\left[\frac{u^{\psi,\text{old}}}{|\nabla\psi_1|}(\sin\theta_1\sin\theta_2 + \cos\theta_1\cos\theta_2\cos\Delta\zeta) + \frac{u^{\theta,\text{old}}}{|\nabla\theta_1|}(\cos\theta_1\sin\theta_2 - \sin\theta_1\cos\theta_2\cos\Delta\zeta) + \frac{u^{\zeta,\text{old}}}{|\nabla\zeta_1|}\cos\theta_2\sin\Delta\zeta\right], \tag{26}$$

$$u^{\theta,\text{new}} = |\nabla\theta_2|\left[\frac{u^{\psi,\text{old}}}{|\nabla\psi_1|}(\sin\theta_1\cos\theta_2 - \cos\theta_1\sin\theta_2\cos\Delta\zeta) + \frac{u^{\theta,\text{old}}}{|\nabla\theta_1|}(\cos\theta_1\cos\theta_2 + \sin\theta_1\sin\theta_2\cos\Delta\zeta) - \frac{u^{\zeta,\text{old}}}{|\nabla\zeta_1|}\sin\theta_2\sin\Delta\zeta\right], \tag{27}$$

$$u^{\zeta,\text{new}} = |\nabla\zeta_2|\left[-\frac{u^{\psi,\text{old}}}{|\nabla\psi_1|}\cos\theta_1\sin\Delta\zeta + \frac{u^{\theta,\text{old}}}{|\nabla\theta_1|}\sin\theta_1\sin\Delta\zeta + \frac{u^{\zeta,\text{old}}}{|\nabla\zeta_1|}\cos\Delta\zeta\right]. \tag{28}$$

For a concentric circular cross-section tokamak, the preceding three equations can be used to compute the $v^{\alpha_i t+\Delta t}$ and $\tilde{u}^{\alpha_i t+\Delta t}$ in the Eqs. (19) and (20), respectively. For non-circular cross-section tokamaks, one needs to resort to Eq. (21) for a general treatment.

We note that there are other extensions of Boris by converting the particle position and velocity to the Cartesian coordinates at the beginning of the each step and transforming them back to the magnetic coordinates at the end of the time step,[17,18] where forward and inverse mappings are required between the two sets of coordinates. Here we developed a new approach to extend the Boris algorithm in the complex tokamak magnetic field without using the inverse mapping of the coordinates. In addition, this new method is completely compatible with the current numerical equilibrium model used in the GTC code[5] and can extend the original code naturally to include full particle orbit simulations.

IV. SIMULATION RESULTS

The new algorithm has been implemented first in a full kinetic code and then incorporated to the gyrokinetic toroidal code GTC. Several simulations for the charged particle dynamics in tokamaks have been carried out by this full kinetic code to demonstrate the validity and usefulness of this new Boris algorithm in magnetic coordinates. The typical orbits for trapped and passing particles are shown in the left panels of Fig. 2. The right panels show the poloidal projection of the particles on the R-Z plane. The full particle orbits are closed loops on the R-Z plane after several hundred gyro-

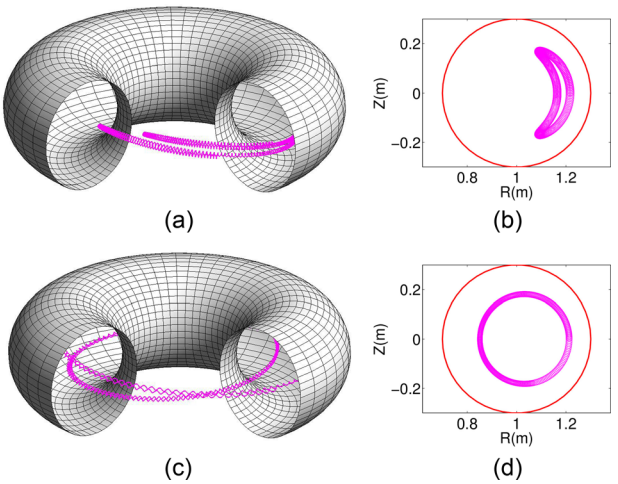

FIG. 2. (a) Orbit of a trapped particle in the tokamak. (b) Projection of the trapped orbit on the R-Z plane. (c) Orbit of a passing particle. (d) Projection of the passing orbit on the R-Z plane. The projected orbit is closed during several bounce or transit periods.

periods as predicated by the analytical theory, which indicates good numerical conservation properties for this new algorithm. Although there is a coordinate transformation in every time step, this new algorithm does not lose accuracy in the long time scale.

As a comparison, the 4th order Runge-Kutta algorithm (RK4) is also employed to simulate the particle orbit in the tokamak. Fig. 3 shows the time history for the kinetic energy E_k and magnetic moment μ for Boris algorithm and RK4, respectively, where the kinetic energy $E_k = \frac{1}{2}mv^2$ and magnetic moment $\mu = \frac{mv_\perp{}^2}{2B}$ are calculated from the velocity of the particle and local geometrical information at each time step. As seen in Fig. 3, for the same time step size $\Delta t = 1/32T_c$ with $T_c = 2\pi/\Omega$, the RK4 algorithm fails to conserve kinetic energy and magnetic moment, while the Boris algorithm conserves kinetic energy and magnetic moment for more than one thousand gyro-periods. Since the magnetic field is static and no electric field is invoked, only the direction of the particle velocity changes at each time step in the Boris scheme, which leads to a perfect conservation of the kinetic energy. The magnetic moment μ in long time simulation shows variation at three different time scales. First in the fastest time scale, the magnetic moment oscillates with the gyromotion. Second, the magnetic moment oscillates in the slower bounce time scale. Third, at an even longer time

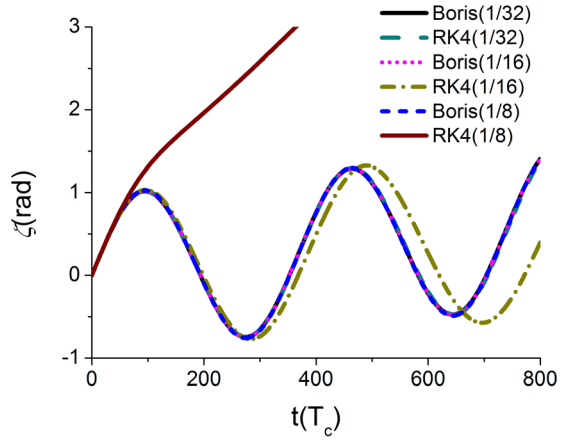

FIG. 4. Time history of the toroidal angle of the particle using different time step sizes.

scale the magnetic moment decreases very slowly due to the numerical dissipation.

To test the convergence of this algorithm, we carry out several simulations using different time step sizes. In Fig. 4, we plot the motion of the particle in the toroidal direction. When $\Delta t = 1/32T_c$, the black solid curve denoting the Boris algorithm overlaps the cyan dashed curve denoting the RK4 algorithm, which shows that these methods converge to the exact particle orbit in the small time step size limit as is expected. The RK4 curve begins to deviate from the converged orbit when $\Delta t = 1/16T_c$ and gives a numerically diverged orbit when $\Delta t = 1/8T_c$. However, it is surprising to see that the Boris algorithm maintains adequate accuracy even when $\Delta t = 1/8T_c$. If there are high frequency electromagnetic perturbations, $\omega_{perturb}\Delta t < 1$ will set an upper bound for the time step size.

We also simulate the guiding center orbits with the same parameters. As Fig. 5(a) shows, the guiding center orbit does not match exactly the full particle orbit. Although the same equilibrium magnetic field is used in the guiding center orbit simulation and full particle orbit simulation, there still unavoidably exist some higher order corrections in the ε expansion due to the different formulations for these two algorithms, where ε is the inverse aspect ratio and $\varepsilon \equiv r/R_0$. The difference for the bounce time of a trapped particle between these two simulation methods is calculated and plotted in Fig. 5(b). If the equilibrium magnetic field in guiding center simulation and full particle orbit simulation is accurate to the first order of ε, the difference is found to be

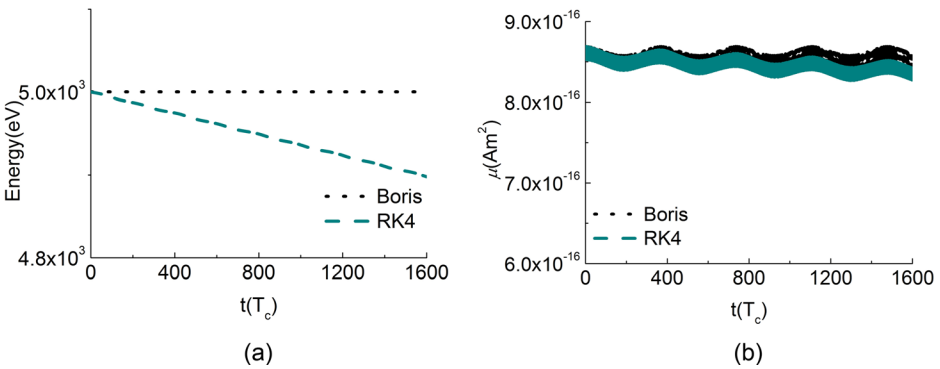

FIG. 3. (a) Time history of the kinetic energy of a particle using the Boris algorithm and the four-order Runge-Kutta algorithm (RK4). (b) Time history of the magnetic moment using the Boris algorithm and RK4 algorithm. The width of the line shows the fluctuation caused by gyro-motion. The simulations last for about four bounce periods.

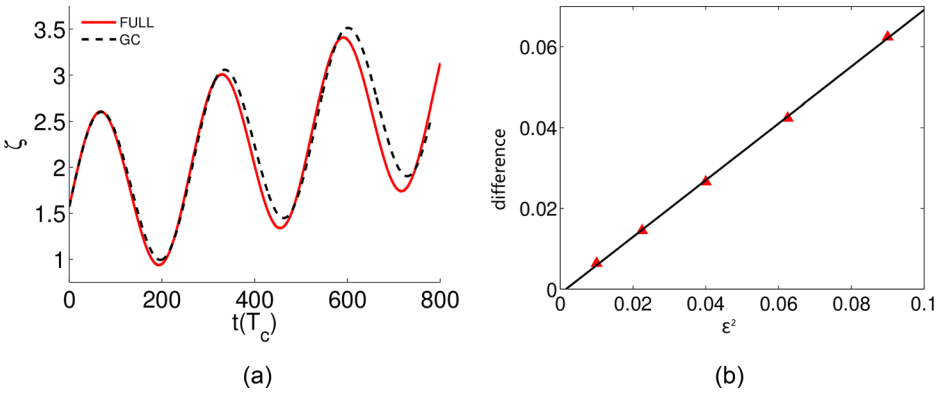

FIG. 5. (a) Time history of the toroidal angle of a trapped particle from full kinetic (FULL) simulation and guiding center(GC) simulation. (b) The relative difference for the bounce time between the full kinetic simulation and the guiding center simulation. The red markers are from the simulation data, and the black line is a fitted straight line.

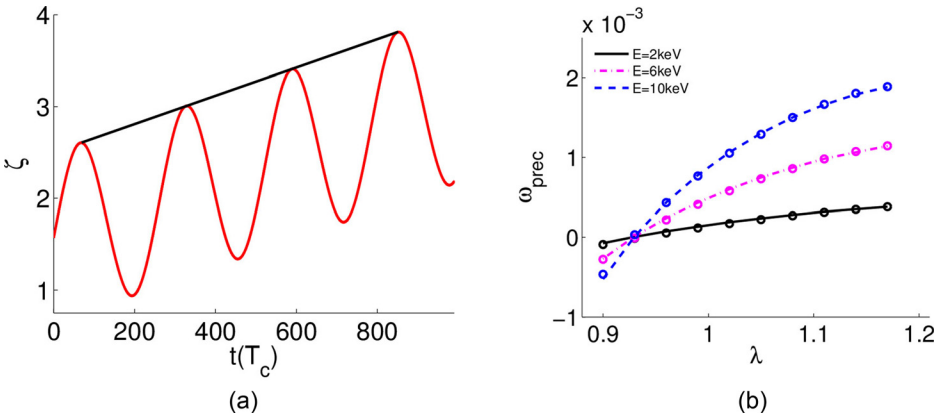

FIG. 6. (a) Calculation of the toroidal precession frequency. The red curve shows the toroidal angle of a trapped particle. The black solid line connects several local maxima, i.e., the banana tips. The slope of the black solid line is the toroidal precession frequency. (b) The toroidal precession frequency of trapped particles vs. pitch angle for different energies: the continuous curves with different colors are from the full particle orbit simulation using the Boris algorithm, and the discrete circular markers are from the guiding center simulation.

proportional to the order of ε^2, as shown by Fig. 5(b). Therefore, the difference between the guiding center and full particle orbits is mainly due to the implementation difference of the equilibrium model, rather than the algorithm itself. In addition, the toroidal precession of trapped particles[20,21] is investigated using both full particle and guiding center simulations. Fig. 6(a) shows the toroidal angle of the particle or the guiding center versus time. The slope of the local maxima gives the toroidal precession speed, which can be used to compute the toroidal precession frequency. The toroidal precession frequencies for different pitch angles are shown in Fig. 6(b) with the normalized pitch angle $\lambda = \mu B_0/E_k$, and B_0 is the magnetic field at the magnetic axis. The continuous curves are from full particle simulation and the discrete circles are from the guiding center simulation. The results from these two methods are consistent with each other, which verifies the ∇B drift and the curvature drift in the Boris scheme. This shows the validity of the Boris algorithm in the very long time scale simulation. With an external poloidal electric field added, the particle will possess a radial $E \times B$ drift, as is verified in Fig. 7.

If there is a toroidal electric field, the Ware pinch[22] can be recovered by the Boris full particle orbit simulation. As illustrated in Fig. 8(a), the projection of the orbit on the R-Z plane is no longer closed and there is a radial drift with the speed $v = E_\phi/B_p$. The radial drift speed of the trapped particle can also be calculated by its orbit, as shown in Fig. 8(b), which matches the theoretical prediction. If a time-dependent radial electric field is introduced, there will be a radial polarization drift proportional to $\frac{\partial E_r}{\partial t}$ given by $v_p = \frac{\varepsilon_0}{ne}\frac{\omega_{pi}^2}{\omega_{ci}^2}\frac{\partial E_r}{\partial t}\frac{B_0^2}{B_p^2}$, which is the neoclassical polarization drift.[23] If a monotonically increasing electric field is applied, i.e., $E_r(t) = E_0 t$, a constant radial polarization drift v_p is observed, as shown in Fig. 9(b). This neoclassical polarization drift can also be computed from the full particle orbit, which matches the theoretical prediction.

V. SUMMARY

In this paper, we have derived a form of the Boris algorithm in the magnetic coordinates to push full particle orbits (i.e., with cyclotron motion) in the toroidal plasmas. The metric tensor and Jacobian both appear in the equations of

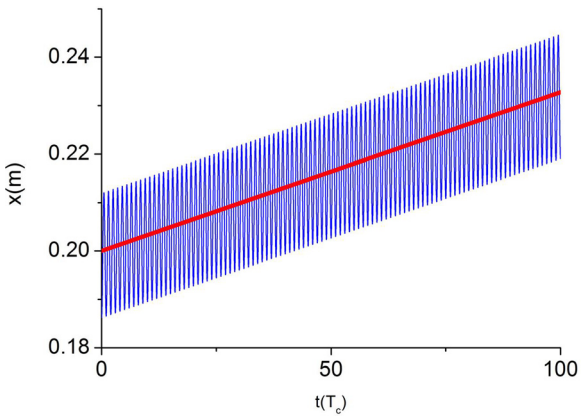

FIG. 7. The motion of a particle in the direction of $\mathbf{E} \times \mathbf{B}$ drift. The blue line is the position of the particle in simulation. The red line is the average drift predicted by theory.

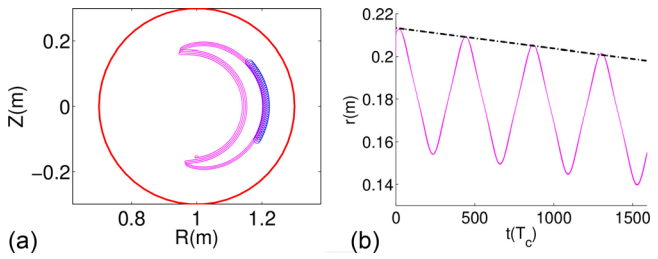

FIG. 8. (a) Ware pinch due to the presence of a toroidal electric field. The magenta solid line is the gyrocenter orbit after smoothing out the particle gyromotion in the full particle simulation. The blue line stands for the full particle orbit during the early phase of the simulation. (b) The radial motion of the gyrocenter (magenta solid line). The black line is the radial drift predicted by the Ware pinch theory.

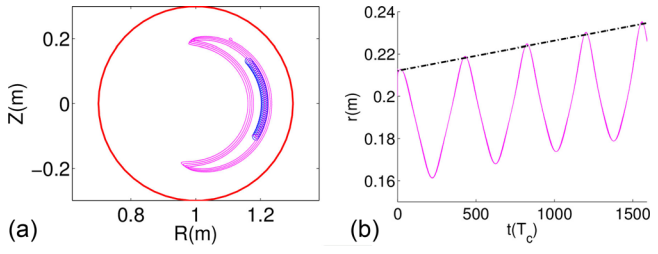

FIG. 9. (a) Neoclassical polarization drift due to an increasing radial electric field. The magenta solid line stands for the gyrocenter orbit after smoothing out the particle gyromotion in the full particle simulation. The blue solid line stands for the full particle orbit during the early phase of the simulation. (b) Radial motion of gyrocenter (magenta line). The black line is the neoclassical polarization drift predicted by theory.

motions to advance the position and velocity, which need to be calculated at the beginning of the simulation. The contravariant component of the velocity needs to be recalculated at each time step to advance the velocity, since the basis vectors at the particle position change as the particle moves. This new algorithm has been implemented to calculate the full particle orbit of the charged particle in a tokamak, recovering faithfully the bounce motion and toroidal precession over a long time period. The kinetic energy and magnetic moment of particle are well conserved in this new algorithm.

The orbit from the full particle simulation using the Boris algorithm overlaps the orbit from the guiding center simulation. Although more computation time is needed for the Boris full particle pushing algorithm compared with the guiding center pushing algorithm, this Boris algorithm is still desirable since it can properly treat the crucial wave-particle interaction in the high frequency wave. With low frequency external electrostatic field, this new Boris algorithm can faithfully recover the well-known physics including toroidal precession, Ware pinch, and neoclassical polarization. Finally, we note that this method and formulation work well not only for the magnetic coordinate system but also for any other curvilinear coordinate system, such as the toroidal coordinates (R, Z, ϕ).

ACKNOWLEDGMENTS

The work was supported by the National Magnetic Confinement Fusion Energy Research Program under Grant Nos. 2015GB110000, 2011GB105001, and 2013GB111000 and, China NSFC under Grant No. 91130031, the Recruitment Program of Global Youth Experts, U.S. DOE SciDAC GSEP centers. The authors thank Professor Liu Chen for useful discussions.

APPENDIX: VOLUME-PRESERVING PROPERTY OF BORIS SCHEME IN MAGNETIC COORDINATES

First, we estimate the error introduced by the approximation in Eq. (18). By Taylor expanding the particle position at time step $t + \Delta t$, we obtain

$$\begin{aligned}\alpha_i^{t+\Delta t} &= \alpha_i^{t+\Delta t/2} + \dot{\alpha}_i^{t+\Delta t/2}\Delta t/2 + 0.5\ddot{\alpha}_i^{t+\Delta t/2}\Delta t^2/4 + \cdots \\ &= \alpha_i^{t+\Delta t/2} + (\mathbf{v}\cdot\mathbf{e}^{\alpha_i})^{t+\Delta t/2}\Delta t/2 \\ &\quad + 0.5(\mathbf{v}\cdot\dot{\mathbf{e}}^{\alpha_i} + \dot{\mathbf{v}}\cdot\mathbf{e}^{\alpha_i})^{t+\Delta t/2}\Delta t^2/4 + \cdots.\end{aligned} \tag{A1}$$

Then we further expand $u^{\alpha_i t+\Delta t}$

$$\begin{aligned}u^{\alpha_i t+\Delta t} &= \mathbf{v}^{t+\Delta t}\cdot\mathbf{e}^{\alpha_i t+\Delta t/2} \\ &= (\mathbf{v}\cdot\mathbf{e}^{\alpha_i})^{t+\Delta t/2} + (\dot{\mathbf{v}}\cdot\mathbf{e}^{\alpha_i})^{t+\Delta t/2}\Delta t/2 + \cdots.\end{aligned} \tag{A2}$$

By substituting Eq. (A2) in Eq. (A1) we find

$$\begin{aligned}\alpha_i^{t+\Delta t} &= \alpha_i^{t+\Delta t/2} + u^{\alpha_i t+\Delta t}\Delta t/2 \\ &\quad + 0.5(\mathbf{v}\cdot\dot{\mathbf{e}}^{\alpha_i} - \dot{\mathbf{v}}\cdot\mathbf{e}^{\alpha_i})^{t+\Delta t/2}\Delta t^2/4 + \cdots.\end{aligned} \tag{A3}$$

Thus Eq. (18) is recovered by keeping the first two terms of Eq. (A3), with an error of order Δt^2.

In Eq. (19), the error only changes the direction of the velocity in the Cartesian coordinate system instead of the magnitude. Therefore, the energy-preserving property is retained.

However, the approximation does not preserve the volume-preserving property precisely. The phase space volume is conserved if

$$dx_k dy_k dz_k dv_k^x dv_k^y dv_k^z = dx_{k+1} dy_{k+1} dz_{k+1} dv_{k+1}^x dv_{k+1}^y dv_{k+1}^z, \tag{A4}$$

where the subscript k means kth time step. The position at kth time step $\mathbf{r}_k = \mathbf{r}(k\Delta t - \Delta t/2)$, and the velocity $\mathbf{v}_k = \mathbf{v}(k\Delta t)$. In the Boris algorithm, the velocity update is a rotation of the velocity vector, which corresponds to a unitary transformation. Therefore

$$dv_{k+1}^x dv_{k+1}^y dv_{k+1}^z = dv_k^x dv_k^y dv_k^z. \tag{A5}$$

However, it is generally difficult to satisfy $dx_{k+1}dy_{k+1}dz_{k+1} = dx_k dy_k dz_k$. For example, one can take $(\alpha_1, \alpha_2, \alpha_3) = (x^2, y, z)$ to show that $dx_{k+1}dy_{k+1}dz_{k+1} \neq dx_k dy_k dz_k$. So the volume-preserving property does not hold in general. However, energy and magnetic moment are well conserved for a long period of time with such an approximation, as shown by our numerical simulation.

[1]C. K. Birdsall and A. B. Langdon, *Plasma Physics via Computer Simulation* (CRC Press, 2004).
[2]R. B. White and M. S. Chance, Phys. Fluids **27**(10), 2455–2467 (1984).
[3]W. W. Lee, Phys. Fluids **26**(2), 556–562 (1983).

[4]H. Qin and X. Guan, Phys. Rev. Lett. **100**(3), 035006 (2008).
[5]Z. Lin, T. S. Hahm, W. W. Lee, W. M. Tang, and R. B. White, Science **281**(5384), 1835–1837 (1998).
[6]A. Kuley, Z. X. Wang, Z. Lin, and F. Wessel, Phys. Plasmas **20**(10), 102515 (2013).
[7]Y. Lin, X. Y. Wang, Z. Lin, and L. Chen, Plasma Phys. Controlled Fusion **47**(4), 657–669 (2005).
[8]Y. Lin, X. Y. Wang, L. Chen, X. Lu, and W. Kong, Plasma Phys. Controlled Fusion **53**(5), 054013 (2011).
[9]Y. Chen and S. E. Parker, Phys. Plasmas **16**(5), 052305 (2009).
[10]J. P. Boris, in *Proceedings of the Fourth Conference on Numerical Simulation on Plasmas* (Naval Research Laboratory, Washington, DC, 1970), pp. 3–67.
[11]L. Patacchini and I. H. Hutchinson, J. Comput. Phys. **228**(7), 2604–2615 (2009).
[12]R. Zhang, J. Liu, H. Qin, Y. Wang, Y. He, and Y. Sun, Phys. Plasmas **22**(4), 044501 (2015).
[13]H. Qin, S. Zhang, J. Xiao, J. Liu, S. Yajuan, and W. M. Tang, Phys. Plasmas **20**(8), 084503 (2013).
[14]S. D. Webb, J. Comput. Phys. **270**, 570–576 (2014).
[15]S. Zhang, Y. Jia, and Q. Sun, J. Comput. Phys. **282**, 43–46 (2015).
[16]Y. He, Y. Sun, J. Liu, and H. Qin, J. Comput. Phys. **281**, 135–147 (2015).
[17]Y. Hu and R. E. Denton, J. Geophys. Res. **114**, A12217, doi:10.1029/2009JA014570 (2009).
[18]M. A. Belyaev, New Astron. **36**, 37–49 (2015).
[19]G. L. Delzanno and E. Camporeale, J. Comput. Phys. **253**, 259–277 (2013).
[20]A. J. Brizard, Phys. Plasmas **18**(2), 022508 (2011).
[21]Y. Xiao and Z. Lin, Phys. Plasmas **18**(11), 110703 (2011).
[22]A. A. Ware, Phys. Rev. Lett. **25**(1), 15–17 (1970).
[23]Y. Xiao, P. J. Catto, and W. Dorland, Phys. Plasmas **14**(5), 055910 (2007).